Research Article

Numerical investigation of a novel solar cell based on a modified perovskite with PPP polymer

S. Yasin [a,*], M. Moustafa [b]

[a] *Physics Program, Department of Mathematics, Statistics, and Physics, College of Arts and Sciences, Qatar University, P.O. 2713, Doha, Qatar*
[b] *Department of Physics, School of Sciences and Engineering, The American University in Cairo, Egypt*

A B S T R A C T

In this paper, a new, highly efficient and eco-friendly solar cell device based on a modified perovskite material from CsMAFA, with a polymer as an absorber layer, is modelled and simulated by utilizing the SCAPS-1D. An encouraging conversion power efficiency of 23.5% is achieved by optimizing several core parameters in the absorber layer and the device structure. The obtained results show remarkable progress in the solar cell performance by increasing the absorber layer's thickness. Indeed, increasing the thickness to 1000 nm is desirable to promote the light absorption process and solar cell efficiency. High doping density in the absorber layer adversely impacted solar cell performance. Additionally, increasing the defect density above 1×10^{16} cm^{-3} yielded a sharp degradation in device performance. This is ascribed to a reduction in the lifetime and the diffusion length of the charge carriers and turned out toward the electron-hole recombination process. Adjusting the electron affinity of the absorber layer at 4.49 eV presented a valued step toward optimizing the device performance through having better band alignment between the layers. The simulations results demonstrated that the device performance starts to be impeded if a metal with a work function less than 5 eV is used as a back contact layer. Finally, the solar cell displayed a continuous degraded behavior with increasing the temperature. The device operates optimally at 300 K. It is believed that this study represents an added value in the field of simulation and fabrication high-efficiency perovskite solar cells and optoelectronic devices.

1. Introduction

Perovskites have been considered promising materials for photovoltaic devices and applications. They exhibit a broadband spectrum absorption, high power conversion efficiency (*PCE*) in their manufactured devices, along with low raw material and preparation costs [1,2]. Since their discovery, perovskite solar cells have attracted the attention among several classes of photovoltaic devices due to the hasty progress in their performance, with a currently certified *PCE* of 25.8% [3]. The remarkable high performance in perovskite solar cells is mainly attributed to the perovskite absorber layer, which represents the core of the solar cell and the harvesting layer for the light absorption process. Several reports have shown that most of the perovskites absorber layer are perfect absorbers for the light, and the absorption process leads to generating charge carriers characterized by long diffusion lengths, which effectively promotes solar cell performance [4,5]. Despite this astonishing progress in the perovskite solar cells performance, many perovskite materials tackle the challenge of expanding their usage in photovoltaic devices. This is due to their unlikely properties, such as being environmentally toxic as in $CH_3NH_3PbI_3$ [6], being unstable in structure as in $CH_3NH_3SnI_3$ [7], and degradation with the environment change as in $CsPbI_3$ [8]. Therefore, searching for new perovskite materials with beloved properties for optoelectronic devices and commercially attractive has expanded enormously through experimental and theoretical research [9–11].

Among several attempts towards improving the physical and chemical properties of perovskite materials toward achieving echo-friendly, highly stable, and enhanced optoelectronic properties, the modified CsMAFA (MA, methylamine cation $CH_3NH_3^+$; FA, formamidinium cation $HC(NH_2)_2^+$) with 3D star-shaped polyhedral oligomeric silsesquioxane-poly (trifluoroethyl methacrylate)-b-poly (methyl methacrylate) (PPP) polymer has appeared recently as a promising candidate for photovoltaic devices [12]. The modified material is distinguished by high structural stability with remarkable photovoltaic properties [12,13]. Experimental results on a solar cell based on this material as an absorber layer reported an extraordinary fill factor of 0.862 with 22.1%

---

* Corresponding author.
  E-mail address: syasin@qu.edu.qa (S. Yasin).

efficiency.

In this study, we present for the first time, to the best of our knowledge, numerical analysis on a new modelled solar cell device based on a modified perovskite material from CsMAFA with a polymer as an absorber layer using the one-dimensional solar cell simulation software (SCAPS-1D) [14]. The implanted modified perovskite material represents a promising candidate as a stable, eco-friendly and economical material for future optoelectronic devices. Thus, the impact of several parameters of the absorber layer, such as the thickness, electron affinity, doping, and defect densities on solar cell performance, is investigated and discussed. To further improve toward achieving a high-performance optoelectronic device, the impact of the back-contact work function and the operating temperature on the efficiency is studied. We believe that this study might pave the way for fabricating high-performance perovskite solar cells.

2. Research methodology

The solar cell modelling and simulation process is crucial before the fabrication process. It represents the base in exploring and understanding the primary performance of the solar cell toward achieving optimal performance. In this paper, we present optoelectronic simulation results on a modelled PPP-modified perovskite (CsMAFA) solar cell for the first time of its kind. The simulation is carried out using the one-dimensional solar cell capacitance simulator (SCAPS-1D) [14]. Several software for solar cell simulation are available such as AMPS-1D for 1D analysis of microelectronic and photonic structures, SimWindows for simulating 1D solar cells and SCAPS-1D. SCAPS-1D has been effectively used in the simulation of several solar cells, e.g., Perovskite, CIGS, CdTe, organic and polymeric-based solar cells. Several reports have shown that SCAPS-1D simulation results have excellent agreement with the existing experimental results. The software represents a professional simulation tool in probing, investigating and giving realistic expectations about the performance of several types of solar cells [15–18]. SCAPS works at different operating conditions with several output parameters, which reflect the device performance. Further details about the basic concepts of SCAPS can be found in our previous publications [19,20].

The modelled perovskite solar cell device and the associated band energy diagram are depicted in Fig. 1. The device is based on the PPP-modified CsMAFA as an absorber layer. The absorber layer is sandwiched by TiO_2 as an electron transport material (ETM) and $MASnBr_3$ (MA = Methyl ammonium) as a hole transport material (HTM) forming the solar cell structure: ITO (window layer)/TiO_2 (ETM)/PPP-modified CsMAFA (absorber layer)/$MASnBr_3$ (HTM)/metal back contact. The modelled device was validated by implementing the preliminary input parameters for all layers selected carefully from several previous studies, as presented in Table 1 [12,21–26]. All simulations are carried out at 300 K and air mass of 1.5 global spectra with a light power of 1000

Table 1
Initial input SCAPS material parameters used for simulation.

Parameters	ITO	TiO_2	modified Perovskite	$MASnBr_3$
Thickness (nm)	300	10	500	10
Band gap (eV)	3.72	3.2	1.59	2.15
Electron affinity (eV)	4.49	4	4.49	3.39
Dielectric Permittivity	9.4	9	6.6	8.2
CB effective density of states (cm^{-3})	4×10^{19}	2×10^{18}	1×10^{19}	1×10^{18}
VB effective density of states (cm^{-3})	1×10^{18}	1.8×10^{19}	1×10^{18}	1×10^{18}
Electron thermal velocity (cm/s)	1×10^7	1×10^7	1×10^7	1×10^7
Hole thermal velocity (cm/s)	1×10^7	1×10^7	1×10^7	1×10^7
Electron mobility (cm^2/V.s)	100	20	14.76	1.6
Hole mobility (cm^2/V.s)	25	10	15.94	1.6
Donor doping concentration (cm^{-3})	1×10^{21}	2×10^{19}	0	0
Acceptor doping concentration (cm^{-3})	0	0	1×10^{15}	1×10^{18}
Defect density N_t (cm^{-3})	1×10^{14}	1×10^{14}	1×10^{14}	1×10^{18}

W/m^2. Besides the parameters listed in Table 1, the interfaces between the layers are also considered in the proposed device with the following parameters for the interfaces TiO_2/PPP-modified CsMAFA and PPP-modified CsMAFA/$MASnBr_3$: neutral defect type, single energetic distribution, the energy level of 0.6 eV with respect to the valence band (E_v), and capture cross-section of 1×10^{15} cm^2 for the electron and hole. A back contact work function of 5.5 eV is adopted in the simulations.

The modelled solar cell and its initial performance are validated, analyzed, and compared with previous experimental and theoretical studies. As shown in Fig. 2, the short-current density (J_{SC}) hits a value of 22.48 mA/cm^2, while the quantum efficiency (QE) touch the 100% level, indicating high absorption and generation processes in the solar cell device. The initial performance parameters yielded a PCE of 18.38%, open-circuit voltage (V_{OC}) of 0.95 V, and fill factor (FF) of 86.11%. The obtained results are consistent with recent studies on perovskite solar cells [12,27].

For high-performance solar cells, careful investigation for the absorber layer parameters such as thickness, electron affinity, and defect density is performed. In addition, the back-contact work function and the operating temperature are considered for further solar cell optimization. The impact of each parameter on the solar cell performance is analyzed and discussed.
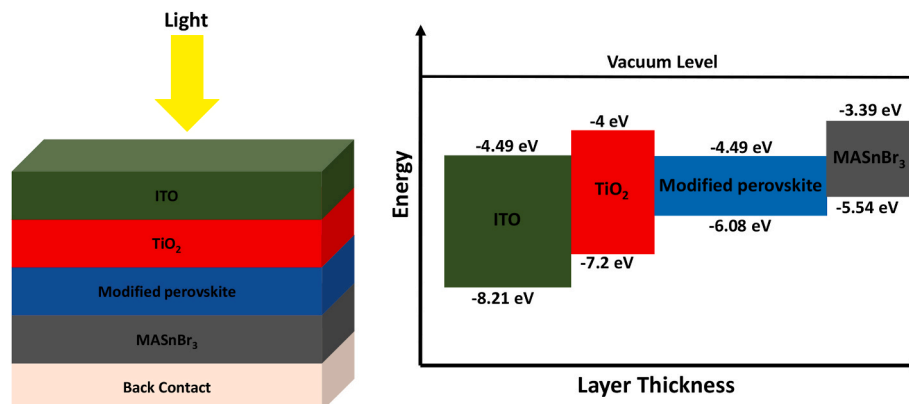
Fig. 1. Schematic diagram of the modelled solar cell and the corresponding energy band diagram.
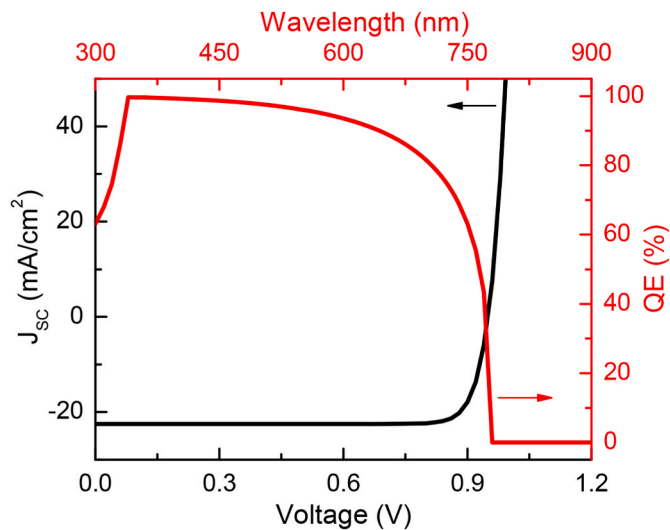
Fig. 2. (Colour online) The obtained Quantum efficiency QE (red line) and J-V (black line) characteristics at the initial solar cell parameters input.

3. Results and discussion

3.1. Effect of the absorber layer thickness

The absorber layer is the central layer in the structure of solar cells. Its role is essential in figuring out the performance of the solar cell. In this layer, most optical processes, including absorption of the spectrum and generation of the charge carriers, occur. These processes are strongly affected by the physical properties of the absorber layer, such as the energy bandgap, electron affinity and defect density. Noticeably, the efficiency of photons absorption and exciting electron-hole pairs are strongly associated with the thickness of the absorber layer [19,28,29]. The thickness of the absorber layer directly impacts the diffusion length of the photogenerated charge carriers. It promotes the diffusion lengths to higher values due to absorbing a large number of photons. However, increasing the thickness excessively could reverse the solar cell performance due to the adverse saturation current. To explore the optimum performance for the solar cell, the thickness of the modified perovskite layer was studied. Fig. 3(a–d) shows the simulated results of the performance parameters for varying the absorber layer thickness from 100 nm to 1000 nm. All parameters except the FF continuously increase with a saturation feature above 800 nm as the thickness increases. An optimal *PCE* of 19.98% is found at 1000 nm.

Increasing J_{SC} with increasing the thickness can be discussed as follow. As the thickness of the perovskite absorber layer increases, more light will be absorbed by the layer, leading to more of the generated electron-hole pairs, causing the J_{SC} to increase. Increasing the V_{OC} with increasing the thickness can be understood by recalling the equation below [30]:

$$V_{OC} = V_0 \ln\left(\frac{I_L}{I_0} + 1\right) \tag{1}$$

where V_0 is the thermal voltage, I_L is the photogenerated current and I_0 is the dark saturation current. The dark saturation current is a measure of the electron-hole recombination in the solar cell. Increasing the thickness leads to having more charge carriers with longer diffusion lengths that can reach the back contact, thus higher I_L, and simultaneously less electron-hole recombination, which keeps I_0 depressed to a low level, and enhances the V_{OC}. The continuous drop in the FF could be
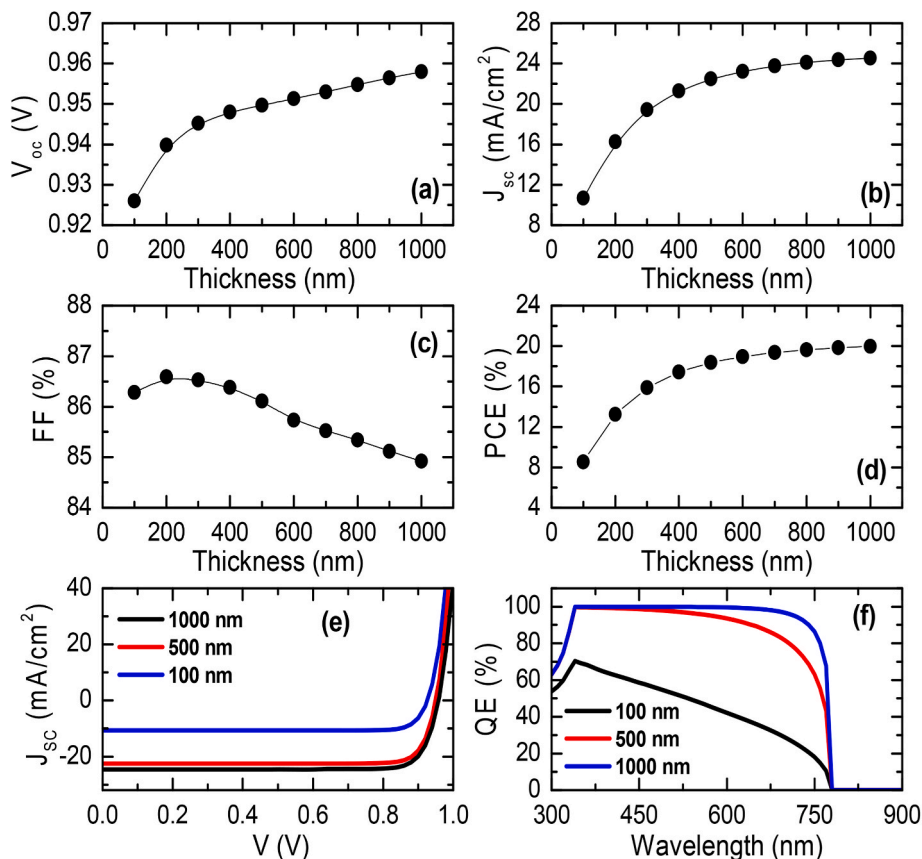
Fig. 3. (a–d) Effect of the modified perovskite absorber layer thickness on the solar cell simulated parameters. (e–f) J-V and Quantum efficiency (QE) characteristics with various absorber layer thicknesses.

argued to increase the series resistance and internal power depletion that elevate by the thickness increase. The positive impact of increasing the absorber layer thickness on the solar cell performance can also be observed in the short-current density (J_{SC}) and quantum efficiency (QE) behaviours (Fig. 2(e–f)). The J_{SC} increases from 10.7 mA/cm^2 at 100 nm to 24.6 at 1000 nm. The QE jumps from 65% at 10 nm to hit the 100% level at 1000 nm. This drastic increase in the J_{SC} and QE with increasing the thickness is an explicit indication for the positive contribution for the absorber layer thickness in promoting the light absorption process, hence enhancing the device performance.

3.2. Effect of the absorber layer doping density

The doping level of the absorber layer is one of the key parameters for promoting the performance of the solar cell. Indeed, it has a direct impact on the mobility of the charge carriers. In general, increasing the doping density creates a depletion region in the structure, forming a built-in voltage area [31,32]. This built-in voltage works as a trapping centre for the charge carriers and obstructs them from reaching the back contact. For low doping levels, the built-in voltage has a weak effect on the mobility of the charge carriers. On the other hand, its effect becomes significant and more pronounced on mobility and at high levels. Several studies have reported that increasing the doping density to high levels cause a deficiency in solar cell performance [20,25,33,34]. To explore this effect on our modelled device, the doping density of the absorber layer was varied from 1×10^{14} cm^{-3} to 6×10^{19} cm^{-3}. As shown in Fig. 4, the efficiency of the solar cell increases smoothly with increasing the doping density up to 3×10^{19} cm^{-3} reaching the highest PCE of 23.92%. Further increase in the doping density beyond 3×10^{19} cm^{-3} led to a considerable degradation in the device performance. A sharp drop in the efficiency is observed, which can be attributed directly to the trapping electric field induced by the built-in voltage in the depletion region.

3.3. Effect of the absorber layer defect density

Defects are inevitable in perovskites. They can be found in the form of point and Frenkel defects [26]. Y. M. Lee et al. reported that advanced defects like dislocations and grain boundaries might also exist in perovskites [35]. Recent studies have shown that the quality of the perovskite absorber layer is crucial for solar cell performance through its impact on the charge carriers' lifetime and the diffusion length [15,31, 36,37]. A high defect density level in the absorber layer accelerates the recombination process in the absorber layer and prevents the
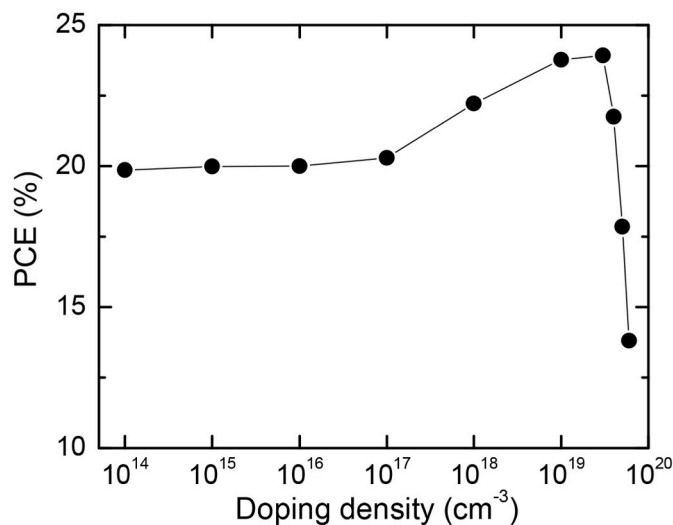
Fig. 4. Effect of the doping density of the modified perovskite absorber layer on the power conversion efficiency (*PCE*) of the solar cell.

photogenerated carriers from reaching the metal back contact. Therefore, having a high-quality perovskite absorber layer through adjusting the defect density to a favorable level is indispensable for achieving high-performance solar cells. In this study, for having a realistic solar cell device, the impact of the defect density of the absorber layer on the device performance via simulation is investigated by varying the defect density from 1×10^{14} cm^{-3} to 1×10^{18} cm^{-3}. As depicted in Fig. 5, the defect density affects all the photovoltaic parameters. The device displays a stable performance of up to 1×10^{16} cm^{-3}, which is a desirable property for the experimental preparation. The device shows the highest performance at a defect density of 1×10^{14} cm^{-3} with PCE of 23.92%, J_{SC} of 19.98 mA/cm^2, V_{OC} of 1.35 V, and FF of 88.9%. Deeping the defect density in the absorber layer to be larger than 1×10^{16} cm^{-3} leads to a breakdown in the performance of the solar cell, where all parameters decrease sharply with the increase of the defect density, and the PCE drops to a value of 4.51% at a defect density of 1×10^{18} cm^{-3}. This drastic decrease in the solar cell performance at high doping level (above 1×10^{16} cm^{-3}) indicates that the recombination rate of the charge carriers is dominant at this stage, and less number from the photogenerated charge carriers are able to reach the back contact due to the reduction in their lifetime and diffusion length.

For further investigation of the impact of the defect density of the absorber layer on the photogenerated charge carriers' lifetime and diffusion length, and consequently, the solar cell performance, Shockley-Read-Hall recombination model (SRH) is recalled [39,40]. According to this model, the lifetime $\tau_{n,p}$ and the diffusion length $L_{n,p}$ for the photogenerated charge carriers (electrons and holes) are expressed by [25,38].

$$\tau_{n,p} = \frac{1}{\sigma_{n,p} \cdot v_{th} \cdot N_t} \tag{2}$$

$$L_{n,p} = \sqrt{\frac{\mu_{n,p} k_B T}{q} \tau_{n,p}} \tag{3}$$

where $\sigma_{n,p}$ is the capture cross-section area for the electrons and holes. v_{th} is the thermal velocity $N_{n,p}$ is the density of trap defect, $\mu_{n,p}$ is the electron and hole mobility, and q is the carrier charge. Table 2 lists the calculated values for the lifetime and diffusion lengths of the electrons and holes using equations (2) and (3) for different defect densities. It can be concluded directly from the calculated values that the lifetime becomes smaller with increasing the defect density due to increased recombination rate, which implies a reduction in the diffusion length. Hence, a deterioration in the solar cell performance.

3.4. Influence of the electron affinity

Band alignment between ETM/Absorber and Absorber/HTM layers is an essential factor in enhancing the performance of the solar cell. It has a significant impact in smoothing charge carriers' movement through the layers toward the metal back contact [36,37]. In addition, it helps in reducing the recombination rate at the interfaces and promotes the photogenerated charge carriers' extraction process. Band alignment optimization in the solar cell can be done by selecting appropriate ETM, and HTM layers or optimizing the valence band offset (VBO) and conduction band offset (CBO) of the absorber layer. The last one can be investigated by tuning the electron affinity of the absorber layer. In this study, we studied the effect of the electron affinity of the absorber layer on the PCE. The electron affinity was varied from 3.7 eV to 4.6 eV. As shown in Fig. 6, the PCE increases noticeably with increasing the electron affinity. At an electron affinity of 4.49 eV, the solar cell displays the best performance with PCE of 23.5%. Increasing the electron affinity beyond 4.49 eV implied a drastic change in the PCE. It drops sharply with a further increase in the electron affinity. Increasing the solar cell performance with increasing the electron affinity can be argued to
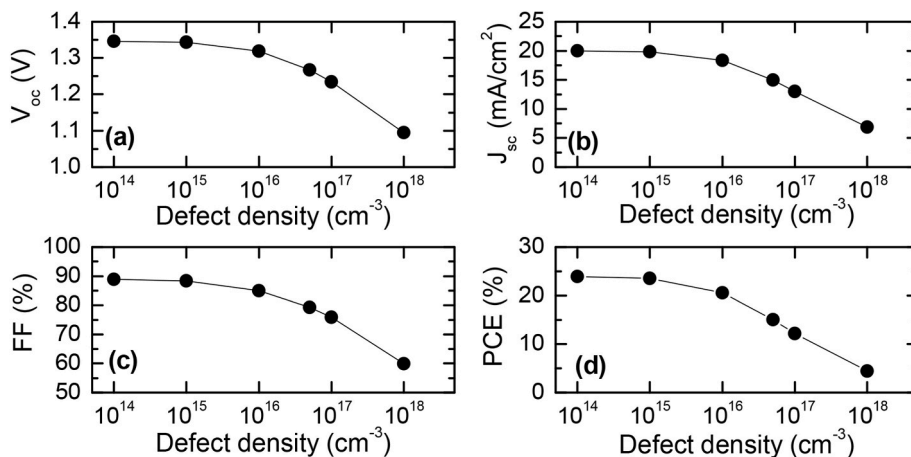
Fig. 5. (a–d) Effect of the modified perovskite absorber layer defect density on the solar cell simulated parameters.

Table 2
Variations of the lifetime and diffusion length for the electrons and holes with defect density in the absorber layer. The value of efficiency is included for comparison.

| Defect density N_t (cm^{-3})	1×10^{14}	1×10^{15}	1×10^{16}	5×10^{16}	1×10^{17}	1×10^{18}
τ_n (s)	3.7×10^{-5}	3.7×10^{-6}	3.7×10^{-7}	7.3×10^{-8}	3.7×10^{-8}	3.7×10^{-9}
τ_p (s)	3.5×10^{-5}	3.5×10^{-6}	3.5×10^{-7}	7×10^{-8}	3.5×10^{-8}	3.5×10^{-9}
L_n (m)	3.76×10^{-5}	1.19×10^{-5}	3.76×10^{-6}	1.67×10^{-6}	1.19×10^{-6}	3.76×10^{-7}
L_p (m)	3.8×10^{-5}	1.2×10^{-5}	3.8×10^{-6}	1.7×10^{-6}	1.2×10^{-6}	3.8×10^{-7}
PCE (%)	23.92	23.50	20.55	12.18	15.03	4.51
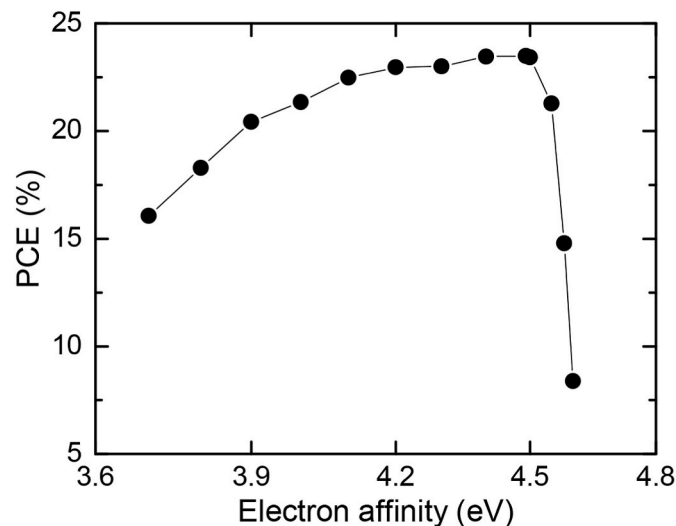
Fig. 6. Effect of the electron affinity of the modified perovskite absorber layer on the power conversion efficiency (PCE) of the solar cell.

inhabitation in the interface recombination induced by an unfavourable mismatch between the energy bands of the layers. At high electron affinity, the interface becomes an obstacle for extracting the charge carriers from reaching the back contact layer leading to a degradation in the solar cell performance.

It is interesting to mention that the TiO$_2$ layer (energy gap of 3.2 eV) absorbs photons of nearly ultraviolet wavelengths to produce electron–hole pairs, while PPP-modified CsMAFA is expected to absorb photons of longer wavelengths due to the small energy bandgap. Our simulation declared that removing the TiO$_2$ layer results in an open-circuit solar cell behavior even though the matching level of the conduction band between ITO and perovskite. This could be inappropriate misalignment between the energy band levels. Since the recombination of the charge carriers is harmful to the solar cell performance, optimizing the valence band offset (VBO) and conduction band offset (CBO) helps reduce the recombination rate and enhance the charge carriers' extraction. Optimizing the offsets can be done by varying the electron affinity of the ITO or the perovskite. We found that reducing the electron affinity of ITO to 4.2 eV results in efficiency of 18.41% with minor overall effect on the solar cell performance in comparison with the structure including the TiO$_2$ layer. We believe that better optimization of the valence band offset (VBO) and conduction band offset (CBO) could result in higher solar cell performance.

3.5. Effect of different back contact work functions

The back contact work function Φ_m is a crucial parameter in shaping solar cell performance. In general, increasing the back contact work function has positively impacted the photovoltaic properties [24, 40–42]. The Φ_m can be changed in the solar cell based on the selected metal used as a back contact layer. Table 3 shows the list of metals and the corresponding work functions used as a metal back contact in the simulation. As illustrated in Fig. 7, the *PCE* is strongly influenced by increasing the work function. The *PCE* increases from 14.2% for Ag (4.7 eV) to become saturated around 23.5% for Ni (5.5 eV) and Platinum (5.7 eV). The effect of the work function on the solar cell performance is associated with the adjacent layer to the back contact. For an adjacent n-type layer, Φ_m is expressed as [41].

$$\Phi_m = \chi + k_B T \ln\left(\frac{N_C}{N_D + N_A}\right) \tag{4}$$

and if the adjacent layer is a p-type as in our modelled solar cell, Φ_m is expressed as

$$\Phi_m = \chi + E_g - k_B T \ln\left(\frac{N_C}{N_A - N_D}\right) \tag{5}$$

where χ is the electron affinity, E_g is the energy bandgap. N_C is the

Table 3
Different metals and their work functions are used in simulations.

Metal	Ag	Nb	Cu	Au	Ni	Pt
Work function (eV)	4.7	4.87	5	5.1	5.5	5.7
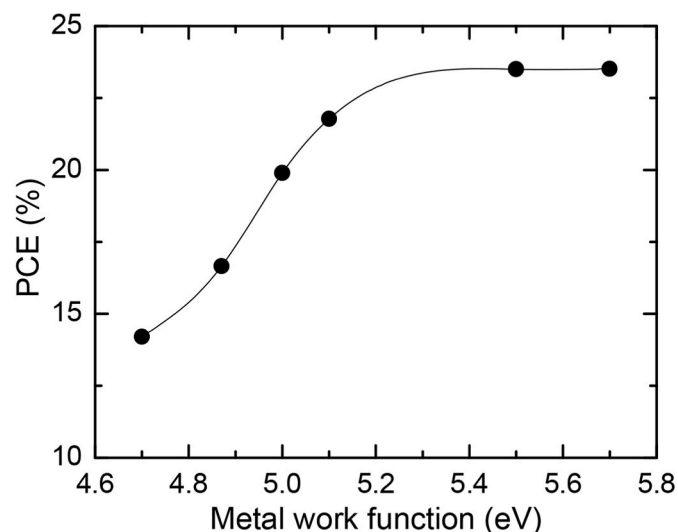
Fig. 7. Effect of the metal work function on the power conversion efficiency (PCE) of the solar cell.

conduction band effective density of states. N_A and N_D are the acceptors and donors concentrations, respectively. Increasing the work function at the junction between the adjacent layer and the metal back contact forces the junction to be more ohmic rather than having Schottky behaviour, implying an increase in the solar cell performance. In MASnBr$_3$, the work function is 4.3 eV [23]. As clear from Fig. 7, the efficiency increases greatly as the metal work function gets far away from the 4.3 eV. This is due to ohmic behavior domination at the MASnBr$_3$/back contact junction, decreasing the energy barrier height for the charge carriers. The optimal performance is observed for the nickel and Platinum ($\Phi_m = 5.5\ eV$ and $5.7\ eV$, respectively) with *PCE* of 23.5%. For economic considerations, nickel could be more attractive than Platinum to be used in solar cells.

3.6. Effect of operating temperature

In general, increasing the operating temperature of the solar cell leads to a negative impact on its performance. Several experimental and theoretical studies have shown that increasing the temperature could deteriorate the solar cell performance [43–45]. This deterioration is argued mainly to the deformation between the solar cell layers, which enhances the interfacial defects between the layers and reduces the diffusion length of the charge carriers, preventing them from reaching the back contact. As a result, a drop in efficiency would be observed. To explore this effect on our modelled device, the temperature was varied from 300 K to 500 K. As shown in Fig. 8, all simulated parameters except
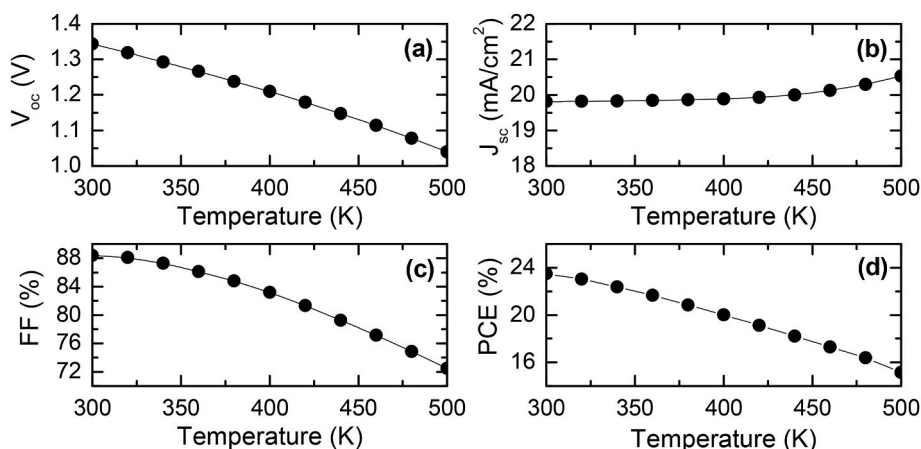
the J_{SC} display a constant diminution with increasing the temperature. The *PCE* decreased from 23.5% to 15.15%. This pronounced drop in efficiency is due to a badly generated interconnectivity between the layers caused by the temperature increase. Increasing the temperature leads to increasing the recombination rate in the absorber layer and thus increase the series resistance of the solar cell. As a consequence, a weak performance in the solar cell. The slight increase of J_{SC} with temperature increase could be due to the weak thermal generation rate of the charge carriers. Since the increasing rate in J_{SC} is much lower than the diminution rate in V_{OC}, a decrease in efficiency is dominant.

4. Conclusions

A new model for a highly efficient solar cell device based on a modified perovskite material from CsMAFA with a polymer as an absorber layer in the structure was simulated by SCAPS-1D. A detailed investigation and discussion on the effect of the absorber layer parameters on the solar cell performance were introduced. The results showed that increasing the thickness of the absorber layer to 1000 nm is desirable to improve the efficiency of the solar cell. High doping in the absorber layer was not beneficial for the device performance, and the optimal performance for the solar cell is found at a doping density of 3×10^{19} cm^{-3}. In addition, the lifetime and the diffusion length of the charge carriers were strongly affected by the defect density in the absorber layer. Both quantities showed a sharp reduction with increasing the defect density above 1×10^{16} cm^{-3}, where the recombination process for the charge carriers was dominant in this stage. Furthermore, the optimal band alignment between the layers is found at an electron affinity of 4.49 eV for the absorber layer. The back-contact work function significantly influenced the solar cell performance, and utilizing metals having high work function as a back contact layer is essential to upgrade the solar cell performance. Finally, operating the solar cell at 300 K is a crucial factor to grantee an optimum performance for the solar cell with *PCE* of 23.5%, V_{OC} of 1.34 V, J_{SC} of 19.8 mA/cm^2 and *FF* of 88.38%.

CRediT authorship contribution statement

S. Yasin: Writing – original draft, supervised the work, contributed to the simulation, Formal analysis. **M. Moustafa:** edited and reviewed the manuscript and contributed to the visualization and validation of the results. All authors provided critical feedback and approved the final version.

Declaration of competing interest

The authors declare that they have no known competing financial interests or personal relationships that could have appeared to influence

Fig. 8. (a–d) Impact of the operating temperature on the solar cell simulated parameters.

the work reported in this paper.

Data availability

Data will be made available on request.

Acknowledgement

The authors are thankful to Marc Burgelman, the electronics and Information Systems (ELIS), University of Gent, Belgium, for providing free access to SCAPS-1D simulation software.

References

[1] B. Turedi, V. Yeddu, X. Zheng, D.Y. Kim, O.M. Bakr, M.I. Saidaminov, Perovskite single-crystal solar cells: going forward, ACS Energy Lett. 6 (2) (2021) 631–642, https://doi.org/10.1021/acsenergylett.0c02573.

[2] Hyun Suk Jung, Nam-Gyu Park, Perovskite solar cells: from materials to devices, Small 11 (1) (2014) 10–25, https://doi.org/10.1002/smll.201402767.

[3] H. Min, D.Y. Lee, J. Kim, G. Kim, K.S. Lee, J. Kim, M.J. Paik, Y.K. Kim, K.S. Kim, M.G. Kim, T.J. Shin, S. Seok, Perovskite solar cells with atomically coherent interlayers on SnO2 electrodes, Nature 598 (2021) 444–450, https://doi.org/10.1038/s41586-021-03964-8.

[4] Bo Wu, Y. Zhou, G. Xing, Q. Xu, H.F. Garces, A. Solanki, T.W. Goh, N.P. Padture, T.C. Sum, Long minority-carrier diffusion length and low surface-recombination velocity in inorganic lead-free CsSnI3 perovskite crystal for solar cells, Adv. Funct. Mater. 27 (7) (2017), 1604818, https://doi.org/10.1002/adfm.201604818.

[5] W. Ning, F. Wang, B. Wu, J. Lu, Z. Yan, X. Liu, Y. Tao, J.M. Liu, W. Huang, M. Fahlman, L. Hultman, T.C. Sum, F. Gao, Long electron–hole diffusion length in high-quality lead-free double perovskite films, Adv. Mater. 30 (20) (2018), 1706246, https://doi.org/10.1002/adma.201706246.

[6] A. Babayigit, D.D. Thanh, A. Ethirajan, J. Manca, M. Muller, H.G. Boyen, B. Conings, Assessing the toxicity of Pb- and Sn-based perovskite solar cells in model organism Danio rerio, Sci. Rep. 6 (2016), 18721, https://doi.org/10.1038/srep18721.

[7] M. Mottakin, K. Sobayel, D. Sarkar, H. Alkhammash, S. Alharthi, K. Techato, Md Shahiduzzaman, N. Amin, K. Sopian, Md Akhtaruzzaman, Design and modelling of eco-friendly CH3NH3SnI3-based perovskite solar cells with suitable transport layers, Energies 14 (2021) 7200, https://doi.org/10.3390/en14217200.

[8] C.C. Boyd, R. Cheacharoen, T. Leijtens, M.D. McGehee, Understanding degradation mechanisms and improving stability of perovskite photovoltaics, Chem. Rev. 119 (2019) 3418–3451, https://doi.org/10.1021/acs.chemrev.8b00336.

[9] I. Mesquita, L. Andrade, A. Mendes, Perovskite solar cells: materials, configurations and stability, Renew. Sustain. Energy Rev. 82 (3) (2018) 2471–2489, https://doi.org/10.1016/j.rser.2017.09.011.

[10] U. Mandadapu, S.V. Vedanayakam, K. Thyagarajan, B.J. Babu, Optimisation of high efficiency tin halide perovskite solar cells using SCAPS-1D, Int. J. Simulat. Process Model. 13 (3) (2018) 221–227, https://doi.org/10.1504/IJSPM.2018.093097.

[11] A. Kheralla, N. Chetty, A review of experimental and computational attempts to remedy stability issues of perovskite solar cells, Heliyon 7 (2) (2021), e06211, https://doi.org/10.1016/j.heliyon.2021.e06211.

[12] Q. Cao, Y. Li, H. Zhang, J. Yang, J. Han, T. Xu, S. Wang, Z. Wang, B. Gao, J. Zhao, X. Li, X. Ma, S.M. Zakeeruddin, W.E.I. Sha, X. Li, M. Grätzel, Efficient and stable inverted perovskite solar cells with very high fill factors via incorporation of star-shaped polymer, Sci. Adv. 7 (2021), https://doi.org/10.1126/sciadv.abg0633 eabg0633.

[13] M.I. Saidaminov, J. Kim, A. Jain, R.Q. Bermudez, H. Tan, G. Long, F. Tan, A. Johnston, Y. Zhao, O. Voznyy, E.H. Sargent, Suppression of atomic vacancies via incorporation of isovalent small ions to increase the stability of halide perovskite solar cells in ambient air, Nat. Energy 3 (2018) 648–654, https://doi.org/10.1038/s41560-018-0192-2.

[14] M. Burgelman, P. Nollet, S. Degrave, Modelling polycrystalline semiconductor solar cells, Thin Solid Films 361–362 (2000) 527–532, https://doi.org/10.1016/S0040-6090(99)00825-1.

[15] S. Yasin, T. Al Zoubi, M. Moustafa, Design and simulation of high efficiency lead-free heterostructure perovskite solar cell using SCAPS-1D, Optik 229 (1–10) (2021), 166258, https://doi.org/10.1016/j.ijleo.2021.166258.

[16] Sachchidanand, V. Garg, A. Kumar, P. Sharma, Numerical simulation of novel lead-free Cs3Sb2Br9 absorber-based highly efficient perovskite solar cell, Opt. Mater. 122 (A) (2021), 111715, https://doi.org/10.1016/j.optmat.2021.111715.

[17] M. Moustafa, T. Alzoubi, Effect of the n-MoTe2 interfacial layer in cadmium telluride solar cells using SCAPS, Optik 170 (2018) 101–105, https://doi.org/10.1016/j.ijleo.2018.05.112.

[18] H. Heriche, Z. Rouabah, N. Bouarissa, New ultra-thin CIGS structure solar cells using SCAPS simulation program, Int. J. Hydrogen Energy 42 (15) (2017) 9524–9532, https://doi.org/10.1016/j.ijhydene.2017.02.099.

[19] S. Yasin, Z. Abu Waar, T. Al Zoubi, M. Moustafa, Optoelectronic simulation of a high efficiency C2N based solar cell via buffer layer optimization, Opt. Mater. 119 (1–9) (2021), 111364, https://doi.org/10.1016/j.optmat.2021.111364.

[20] S. Yasin, M. Moustafa, T. Al Zoubi, G. Laouini, Z. Abu Waar, High efficiency performance of eco-friendly C2N/FASnI3 double-absorber solar cell probed by numerical analysis, Opt. Mater. 122 (1–7) (2021), 111743, https://doi.org/10.1016/j.optmat.2021.111743.

[21] S.M. Seck, E.N. Ndiaye, M. Fall, S. Charvet, Study of efficiencies CdTe/CdS photovoltaic solar cell according to electrical properties by scaps simulation, Nat. Resour. 11 (2020) 147–155, https://doi.org/10.4236/nr.2020.114009.

[22] G. Kartopua, B.L. Williams, V. Zardetto, A.K. Gürlek, A.J. Clayton, S. Jones, W.M.M. Kessels, M. Creatore, S.J.C. Irvine, Enhancement of the photocurrent and efficiency of CdTe solar cells suppressing the front contact reflection using a highly-resistive ZnO buffer layer, Sol. Energy Mater. Sol. Cell. 191 (2019) 78–82, https://doi.org/10.1016/j.solmat.2018.11.002.

[23] M.C. Jung, S.R. Raga, Y. Qi, Properties and solar cell applications of Pb-free perovskite films formed by vapor deposition, RSC Adv. 6 (2016) 2819–2825, https://doi.org/10.1039/C5RA21291J.

[24] Y. Gan, X. Bi, Y. Liu, B. Qin, Q. Li, Q. Jiang, P. Mo, Numerical investigation energy conversion performance of tin-based perovskite solar cells using cell capacitance simulator, Energies 13 (1–17) (2020) 5907, https://doi.org/10.3390/en13225907.

[25] F. Baig, Y.H. Khattak, B. Mari, S. Beg, A. Ahmed, K. Khan, Efficiency enhancement of CH3NH3SnI3 solar cells by device modeling, J. Electron. Mater. 47 (2018) 5275–5282, https://doi.org/10.1007/s11664-018-6406-3.

[26] P.K. Patel, Device simulation of highly efficient ech-friendly CH3NH3SnI3 perovskite solar cell, Sci. Rep. 11 (2021) 3082, https://doi.org/10.1038/s41598-021-82817-w.

[27] G.M. Arumugam, S.K. Karunakaran, C. Liu, C. Zhang, F. Guo, S. Wu, Y. Mai, Inorganic hole transport layers in inverted perovskite solar cells: a review, Nano Select 3 (2021) 1081–1116, https://doi.org/10.1002/nano.202000200.

[28] E. Karimi, S.M.B. Ghorashi, Investigation of the influence of different hole-transporting materials on the performance of perovskite solar cells, Optik 130 (2017) 650–658, https://doi.org/10.1016/j.ijleo.2016.10.122.

[29] S.I. Uddin, M. Tahir, F. Aziz, M.R. Sarker, F. Muhammad, D.N. Khan, S.H.M. Ali, Thickness optimization and photovoltaic properties of bulk heterojunction solar cells based on PFB–PCBM layer, Energies 13 (1–11) (2020) 5915, https://doi.org/10.3390/en13225915.

[30] K. Tan, P. Lin, G. Wang, Y. Liu, Z. Xu, Y. Lin, Controllable design of solid-state perovskite solar cells by SCAPS device simulation, Solid State Electron. 126 (2016) 75–80, https://doi.org/10.1016/j.sse.2016.09.012.

[31] J.S. Park, S. Kim, Z. Xie, A. Walsh, Point defect engineering in thin-film solar cells, Nat. Rev. Mater. 3 (2018) 194–210, https://doi.org/10.1038/s41578-018-0026-7.

[32] M.D. McCluskey, A. Janotti, Defects in semiconductors, J. Appl. Phys. 127 (1–3) (2020), 190401, https://doi.org/10.1038/s41578-018-0026-7.

[33] G.Y. Fan, D.H. Jing, L.N. Nan, Y. Lei, Z.C. Yu, Effect of carrier mobility on performance of perovskite solar cells, Chin. Phys. B 28 (4) (2019), 048802, https://doi.org/10.1088/1674-1056/28/4/048802.

[34] V.A. Trukhanov, V.V. Bruevich, D. Yu Paraschuk, Effect of doping on performance of organic solar cells, Phys. Rev. B 84 (2011), 205318, https://doi.org/10.1103/PhysRevB.84.205318.

[35] Y.M. Lee, I. Maeng, J. Park, M. Song, J.H. Yun, M.C. Jung, M. Nakamura, Comprehensive understanding and controlling the defect structures: an effective approach for organic-inorganic hybrid perovskite-based solar-cell application, Front. Energy Res. 6 (2018) 1–9, https://doi.org/10.3389/fenrg.2018.00128.

[36] K.W. Kemp, A.J. Labelle, S.M. Thon, A.H. Ip, I.J. Kramer, S. Hoogland, E.H. Sargent, Interface recombination in depleted heterojunction photovoltaics based on colloidal quantum dots, Adv. Energy Mater. 3 (2013) 917–922, https://doi.org/10.1002/aenm.201201083.

[37] S. Lia, P. Liub, L. Pana, W. Lia, S. Yanga, Z. Shia, H. Guoa, T. Xiaa, S. Zhanga, Y. Chena, The investigation of inverted p-i-n planar perovskite solar cells based on FASnI3 films, Sol. Energy Mater. Sol. Cell. 199 (2019) 75–82, https://doi.org/10.1016/j.solmat.2019.04.023.

[38] W. Shockley, W.T. Read, Statistics of the recombinations of holes and electrons, Phys. Rev. 87 (1952) 835–842, https://doi.org/10.1103/PhysRev.87.835.

[39] C.R. Kagan, D.B. Mitzi, C.D. Dimitrakopoulos, Organic-Inorganic hybrid materials as semiconducting channels in thin-film field-effect transistors, Science 286 (1999) 945–947, https://doi.org/10.1126/science.286.5441.945.

[40] T. Minemoto, M. Murata, Impact of work function of back contact of perovskite solar cells without hole transport material analyzed by device simulation, Curr. Appl. Phys. 14 (2014) 1428–1433, https://doi.org/10.1016/j.cap.2014.08.002.

[41] A. Haddout, A. Raidou, M. Fahoume, Influence of the layer parameters on the performance of the CdTe solar cells, Optoelectron. Lett. 14 (2018) 98–103, https://doi.org/10.1007/s11801-018-7229-4.

[42] A. Raj, M. Kumar, H. Bherwani, A. Gupta, A. Anshul, Evidence of improved power conversion efficiency in lead-free CsGeI3 based perovskite solar cell heterostructure via SCAPS simulation, J. Vac. Sci. Technol. B 39 (1) (2021), https://doi.org/10.1116/6.0000718, 012401 (1-12).

[43] M. Moustafa, T. AlZoubi, S. Yasin, Numerical analysis of the role of p-MoSe2 interfacial layer in CZTSe thin-film solar cells using SCAPS simulation, Optik 247 (1–10) (2021), 167885, https://doi.org/10.1016/j.ijleo.2021.167885.

[44] T. AlZoubi, A. Moghrabi, M. Moustafa, S. Yasin, Efficiency boost of CZTS solar cells based on double-absorber architecture: device modeling and analysis, Sol. Energy 225 (2021) 44–52, https://doi.org/10.1016/j.solener.2021.07.012.

[45] Q. Meng, Y. Chen, Y.Y. Xiao, J. Sun, X. Zhang, C.B. Han, H. Gao, Y. Zhang, H. Yan, Effect of temperature on the performance of perovskite solar cells, J. Mater. Sci. Mater. Electron. 32 (2021) 12784–12792, https://doi.org/10.1007/s10854-020-03029-y.